



Drop-on-Demand Inkjet Drop Control With One-Step Look Ahead Estimation of Model Parameters

Jie Wang D, Student Member, IEEE, and George T.-C. Chiu D, Senior Member, IEEE

Abstract—Applications of drop-on-demand inkjet printing in dosage-matter manufacturing and scalable patterning are attributed to its capacity for producing consistent dosages with high placement accuracy. In practice, with the same drop jetting profile, drop volume and drop jetting velocity are affected by variations in ink properties and environmental conditions. Open-loop calibrations are timeconsuming and contribute to frequent line stoppage or unacceptable product variations. In this work, a two-input twooutput stochastic drop volume and jetting velocity model is derived based on ink jetting calibration data. A control algorithm using drop-image-based one-step look ahead estimation of process model parameters is developed to regulate drop volume and jetting velocity. Boundedness and convergence of the parameter estimation error and stability of the closed-loop system are provided. Experimental results demonstrate a significant reduction to within 1% relative error in the drop volume and jetting velocity using the proposed control algorithm.

Index Terms—Additive manufacturing, inkjet, Kalman filter, process control, stochastic system.

I. INTRODUCTION

XTENDED from its application in digital printing, dropon-demand (DoD) inkjet printing has seen broad applications in depositing functional materials, including pharmaceutical manufacturing, MEMS sensor characterization, electronics fabrication, and scalable patterning of reactive materials [1], [2], [3], [4]. In these applications, accurate and consistent drop volume and high drop placement accuracy are keys to achieve the desired geometry and functionality.

Inkjet drop formation has been well documented in literature [5], [6], [7], [8]. The majority of the work contributes to the understanding of mechanisms and dynamics between the input properties/driving signal and the state/properties of the drop leaving the nozzle. These efforts are essential in developing DoD inkjet nozzles and the resulting printhead assemblies. Commercial inkjet printheads are often given a limited set of

Manuscript received 6 January 2023; revised 26 March 2023; accepted 1 May 2023. Date of publication 15 June 2023; date of current version 16 August 2023. Recommended by Technical Editor S. Jeon and and Senior Editor Q. Zou. (Corresponding author: George T.-C. Chiu.)

The authors are with the School of Mechanical Engineering, Purdue University, West Lafayette IN 47907 USA (e-mail: wang2474@purdue.edu; gchiu@purdue.edu).

Color versions of one or more figures in this article are available at https://doi.org/10.1109/TMECH.2023.3277455.

Digital Object Identifier 10.1109/TMECH.2023.3277455

drop jetting control parameters for users to adjust the jetting waveform to accommodate different ink materials [4], [9], [10], [11]. Many of the manufacturer-provided jetting control parameters are not directly related to the physical parameters used in drop formation models. Tuning accessible control parameters via trial-and-error and designing new parameterized waveforms are two typical approaches used in practice to achieve the desired drop jetting properties [9], [12], [13], [14]. Khalate et al. [15], [16] used an approximated narrow-gap model and an experimentally identified model to optimize parameterized firing waveforms to improve the consistency of drop velocity over a wide range of jetting frequency. Ezzeldin et al. [17] optimized waveform control parameters using experimental measurements in a feedforward fashion to improve drop velocity consistency over a wide jetting frequency range. Other approaches, such as genetic algorithms [18] and root system growth algorithms [19], were used to automate the control parameter tuning process. These open-loop approaches are ineffective in compensating for uncertainties in the printing process, such as variations in nozzle size, pressure and temperature fluctuations, and inconsistent ink properties, which negatively affect the consistency of drop volume and jetting velocity. Nontrivial relative standard deviations (RSDs) of the print results were observed using the same firing waveform [10], [20]. Kiefer et al. [21] noticed that the printed dose varies over time and with different nozzles. Fig. 1 shows the fluctuations in drop volume and drop jetting velocity using the same nozzle with the same firing waveform at different times in the span of two weeks. Wide distributions of drop volume and drop jetting velocity pose a challenge for DoD inkjet printing in high-volume applications where precise dosage and constant jetting velocity are critical for consistent performance.

Real-time feedback was used to improve printing performance under uncertainties. Barton et al. [22] controlled the electric field in electrohydrodynamic jet printing based on the measured change in jetting frequency for uncertainty compensation. Better drop placement and more uniform drop size were reported. A neural network model mapping drop characteristics to drive voltages was proposed in [23]. Although a closed-loop PID control framework was also proposed in [23], no closed-loop experimental validation and analysis were presented. In [24] and [25], based on the identified static mappings between firing waveform control parameters and drop characteristics, a PI controller and a one-step look ahead control strategy were reported to regulate drop characteristics. Although preliminary results

1083-4435 © 2023 IEEE. Personal use is permitted, but republication/redistribution requires IEEE permission. See https://www.ieee.org/publications/rights/index.html for more information.

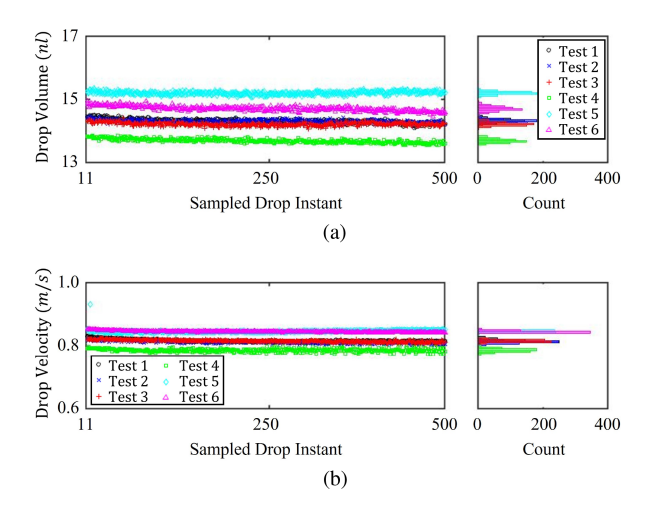


Fig. 1. (a) Drop volumes and (b) jetting velocities using the same nozzle with the same firing waveform at different times in the span of two weeks.

demonstrated the effectiveness of the proposed approaches, analysis of the controlled system was lacking. In this work, an extensive study of the one-step look ahead control strategy for drop characteristics regulation proposed in [25] is provided through detailed analyses of system stability, parameter convergence, output variations, as well as comparison to an integral controller.

The main contributions of this work are given as follows.

- From data collected in a standard printhead-ink calibration process, a two-input two-output static model with parameters characterized by random walks was identified and validated to be a sufficient control-oriented model for regulating drop volume and jetting velocity.
- 2) A control strategy based on one-step look ahead projection-based Kalman estimation of model parameters that can achieve less than 1% RSD regulation performance was introduced and experimentally validated.
- A comprehensive analysis of parameter estimation error bound and convergence and associated closed-loop stability was presented.
- 4) Since the model only requires the accessible control parameters provided by the printhead vendor, it can be readily used to integrate commercial printheads in advanced process control without the need to access internal printhead operations.

The rest of this article is organized as follows. In Section II, the data-based model is developed, followed by the proposed parameter estimation and control strategy and the associated system analysis in Section III. Experimental validation is given in Section IV. Finally, Section V concludes this article.

II. DATA-BASED MODEL DEVELOPMENT

Considering the complexity of first principle based drop formation models and the limited access provided by commercial inkjet printheads to adjust the jetting/firing waveform, a model based on experimental data collected during tuning printhead

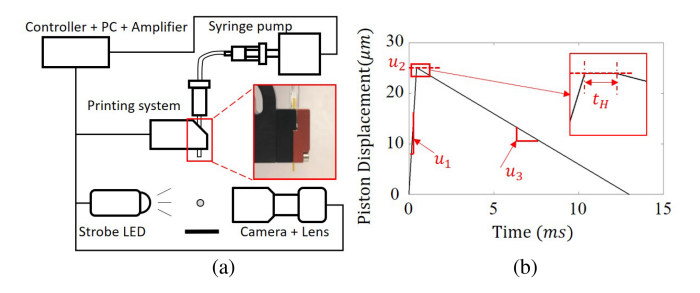


Fig. 2. (a) Schematic of the printing system and (b) a parameterized waveform to PipeJet printhead (BioFluidix PipeJet P9, Freiburg, Germany).

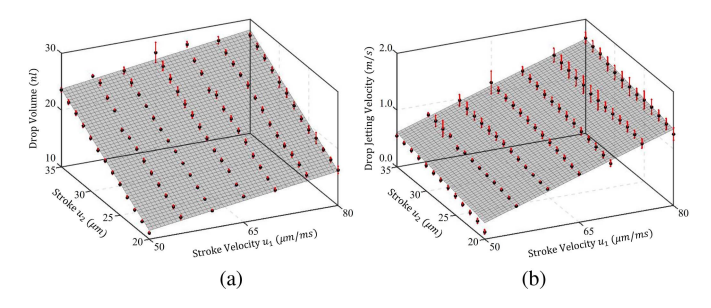


Fig. 3. (a) In flight drop volumes (nl) and (b) jetting velocities (m/s) at different control parameter pairs (u_1, u_2) . Black dots are mean values, red bars denote one standard deviation, and gray planes are the first-order fitting hyperplanes.

firing parameters for a specific ink is employed. Since the printhead tuning experiment and data collection are parts of the standard operating procedure for matching printhead and inks, the proposed modeling approach is applicable to printheads with different jetting mechanisms and with different control parameters for desired drop properties of different inks.

A. Experiments and Data

Using the experimental setup shown in Fig. 2(a) and following the operating procedure in [25] and [26], 91 experiments using a pigment-based black ink without observable abnormal drop jetting behaviors were conducted by varying two user-accessible control parameters of a firing waveform, stroke velocity u_1 and stroke u_2 [see Fig. 2(b)]. In each experiment, at least 200 stroboscopic drop images were captured at the constant control parameter pair (u_1, u_2) .

Using the image processing methods in [24] and [26], in-flight drop volumes and jetting velocities at different (u_1, u_2) were estimated from the stroboscopic drop images and presented in terms of mean and one standard deviation, as shown in Fig. 3. Gray hyperplanes in Fig. 3 are linear least squares regression models based on the 91 experimental data sets using tenfold cross-validation. The data suggest that stroke velocity u_1 has more impact on drop jetting velocity while stroke u_2 mainly controls drop volume, which corresponds to the description in the literature [27] and the printhead datasheet.

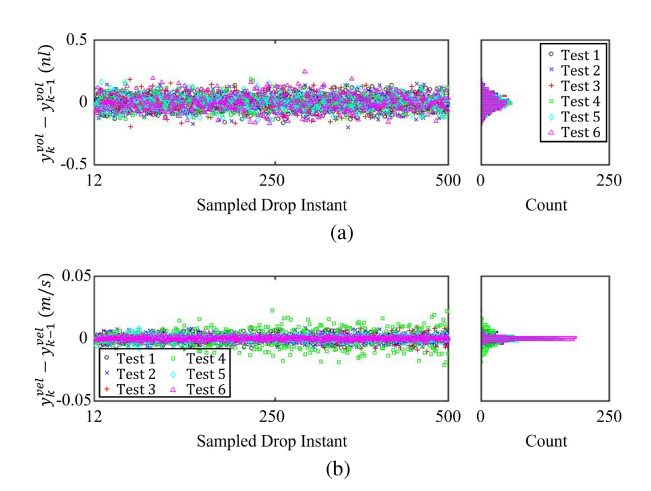


Fig. 4. Output fluctuations $\epsilon_k = Y_k - Y_{k-1}$. (a) Drop volume fluctuations. (b) Drop jetting velocity fluctuations.

B. Drop Volume and Jetting Velocity Model

The data in Fig. 3 suggest that the drop volume y^{vol} and the jetting velocity y^{vel} can be modeled as a two-input two-output static control-oriented model with respect to stroke velocity u_1 , and stroke u_2 , i.e.,

$$Y = \begin{bmatrix} y^{\text{vol}} \\ y^{\text{vel}} \end{bmatrix} = \begin{bmatrix} f_1 \\ f_2 \end{bmatrix} + \begin{bmatrix} g_{11} & g_{12} \\ g_{21} & g_{22} \end{bmatrix} \begin{bmatrix} u_1 \\ u_2 \end{bmatrix} = F + G\bar{U}$$

$$= \begin{bmatrix} 1 & 0 & u_1 & u_2 & 0 & 0 \\ 0 & 1 & 0 & 0 & u_1 & u_2 \end{bmatrix} \begin{bmatrix} f_1 \\ f_2 \\ g_{11} \\ g_{12} \\ g_{21} \\ g_{22} \end{bmatrix} = U\Theta \tag{1}$$

where Y is the output vector, F is the model bias vector, G is the model gain matrix, \bar{U} is the control input vector, U is the input matrix, and Θ is the model parameter vector. Linear least squares regression was used to find the nominal parameters

$$G_o = \begin{bmatrix} 0.15_{(\pm 0.001)} & 0.81_{(\pm 0.002)} \\ 0.035_{(\pm 0.001)} & 0.021_{(\pm 0.002)} \end{bmatrix}$$
 and
$$F_o = \begin{bmatrix} -12.06_{(\pm 0.065)} \\ -1.87_{(\pm 0.067)} \end{bmatrix}$$
 (2)

where the subscripts denote the 95% confidence interval.

To remove different mean values as well as slight drifts shown in Fig. 1, the difference between consecutive outputs in each open-loop test was taken (see Fig. 4), i.e.,

$$\epsilon_k = Y_k - Y_{k-1} = U(\Theta_k - \Theta_{k-1}) \tag{3}$$

where the subscript k is the sampled drop instant and ϵ_k is the consecutive output difference or fluctuation. It can be seen that the consecutive output difference exhibits a zero-mean Gaussian-like distribution, where a random walk model can be used to model the process [28]. Since the drop volume and the

jetting velocity were collected under a constant control input U or equivalently \bar{U} , from (3), we can further represent the parameter fluctuation as a random walk model, i.e.,

$$\Theta_{k+1} = \Theta_k + \mathbf{w}_{k+1} \tag{4}$$

where \mathbf{w}_k is the parameter uncertainty, which may include the effects of changes in ambient conditions and variations in ink properties. With the measurement noise \mathbf{v}_k , (1) becomes

$$Y_k = F_k + G_k \bar{U}_k + \mathbf{v}_k = U_k \Theta_k + \mathbf{v}_k \tag{5}$$

where \mathbf{w}_k and \mathbf{v}_k are assumed to have uncorrelated, zero-mean, Gaussian distributions with covariance matrices Q_k and R_k , respectively. Equations (4) and (5) are the stochastic drop volume and jetting velocity control plant models that will be used for control synthesis in the next section.

Remark 1: A linear model with random parameters is shown to be a reasonable representation for the Pipejet printhead with pigmented ink used in this study. The proposed model structure can be extended to represent other DoD printheads with different nozzle actuations and architectures with different inks, where more complex relationships can be approximated by other representations, such as polynomial models or Gaussian process models.

III. CONTROL STRATEGY

A control algorithm based on one-step look ahead model parameter estimation is proposed because of the importance of the volume and jetting velocity of each discrete in-flight drop for the geometry and functionality of the printed product. Unlike the input matching technique in [29], [30], and [31], the plant model parameter Θ_k fluctuates in a Gaussian distribution fashion as experimentally observed and discussed in the previous section. By leveraging the work done by Zanni et al. [28] and Kiruluta et al. [32], a Kalman estimator is employed to estimate the fluctuating model parameter Θ_{k+1} . A one-step look ahead controller \bar{U}_{k+1} is solved to minimize the expectation value of a cost function comprising the weighted sum of squares of one-step ahead tracking error Ξ_{k+1} and control candidate \overline{U}_{k+1} . The one-step ahead tracking error Ξ_{k+1} is defined as the difference between the desired output Y_d and the estimated system output Y_{k+1} , that is, $\Xi_{k+1} = Y_d - Y_{k+1}$.

Remark 2: In the developed control strategy, regression representation of the plant model equation (5), i.e., $Y_k = U_k \Theta_k + \mathbf{v}_k$, is used for parameter estimation, and the equivalent affine representation $Y_k = F_k + G_k \bar{U}_k + \mathbf{v}_k$ is adopted for controller design. Θ_k as well as its fluctuation equation (4) can be rearranged to these of model gain G_k and model bias F_k , accordingly.

A. Parameter Estimation

By the plant model equation (5), system output Y_{k+1} can be estimated by

$$\hat{Y}_{k+1} = U_{k+1}\hat{\Theta}_{k+1}. (6)$$

 $\hat{\Theta}_{k+1}$ is the estimated model parameter vector computed using the following recursive Kalman update formula:

$$\hat{\Theta}_{k+1} = \hat{\Theta}_k + L_k (Y_k - \hat{Y}_k) = \hat{\Theta}_k + L_k (Y_k - U_k \hat{\Theta}_k)$$
 (7)

where L_k is the Kalman gain ([33], [34]), given by

$$L_k = P_k U_k^T (U_k P_k U_k^T + R_k)^{-1}. (8)$$

In (8), P_k is the covariance matrix of parameter estimation error, $\tilde{\Theta}_k = \Theta_k - \hat{\Theta}_k$, where

$$P_{k+1} = (I - L_k U_k) P_k + Q_{k+1}. (9)$$

To prevent drift in parameter estimation and ensure boundedness of the estimated parameters in the presence of system uncertainty [35], a range of the model parameter Θ can be used as a limit and set to be larger than the confidence interval of the model parameters in (2), i.e.,

$$\theta_k^i \in (\theta_{\min}^i, \theta_{\max}^i), \text{ for } k = 0, 1, \dots$$
 (10)

where θ_k^i is the *i*th entry of the parameter vector Θ_k , which equivalently is the entry of F_k or G_k . Given the parameter range in (10), the parameter updating formula (7) can be modified with a projection operator [36] as follows:

$$\hat{\Theta}_{k+1} = \hat{\Theta}_k + \mathbf{Pr}_{\hat{\boldsymbol{\Theta}}_k} \left(L_k(Y_k - \hat{Y}_k) \right) \tag{11}$$

where

$$\mathbf{Pr}_{\hat{\theta}_{\mathbf{k}}^{i}}\left(\bullet^{i}\right) = \begin{cases} 0 & \text{if } \hat{\theta}_{k}^{i} \geq \theta_{\max}^{i} \text{ and } \bullet^{i} > 0 \\ 0 & \text{if } \hat{\theta}_{k}^{i} \leq \theta_{\min}^{i} \text{ and } \bullet^{i} < 0 \\ \bullet^{i} & \text{otherwise.} \end{cases}$$

Equations (8), (9), and (11) are used to estimate the model parameter Θ at the sampling instant k+1 using the measured output Y_k of the current jetted drop and the associated implemented control input U_k . Knowing Θ_{k+1} , (6) gives the estimated drop volume and jetting velocity at the instant k + 1 for a given control candidate U_{k+1} .

B. Control Design

Given the estimated system output \hat{Y}_{k+1} from (6), a one-step look ahead controller is computed by minimizing the expected value of a cost function that consists of the squared tracking error at the instant k + 1 and the weighted control candidate

$$J = \min_{\bar{U}_{k+1}} E\left[(Y_d - \hat{Y}_{k+1})^T (Y_d - \hat{Y}_{k+1}) + \kappa \bar{U}_{k+1}^T \bar{U}_{k+1} \right]$$
(12)

where $Y_d = [y_d^{\text{vol}} \ y_d^{\text{vel}}]^T, y_d^{\text{vol}}$ is the desired drop volume, y_d^{vel} is the desired drop jetting velocity, and κ is a positive weighting coefficient.

The solution to (12) takes the form

$$\bar{U}_{k+1} = (\hat{G}_{k+1}^T \hat{G}_{k+1} + \kappa I)^{-1} \hat{G}_{k+1}^T (Y_d - \hat{F}_{k+1})$$
 (13)

where \hat{G}_{k+1} and \hat{F}_{k+1} are the estimated model gain and model bias, respectively, which are regrouped from Θ_{k+1} in (11). Note

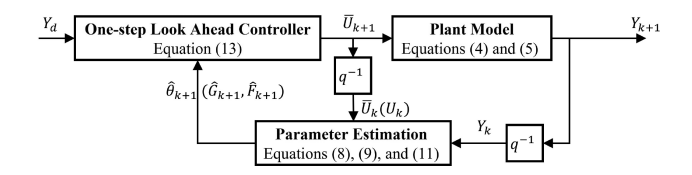


Diagram of the control strategy

that the invertibility of $\hat{G}_k^T \hat{G}_k + \kappa I$ in (13) is ensured by setting

Fig. 5 summarizes the proposed control strategy, where q^{-1} is the one-step delay operator, and (13) is the control law used to control the plant model, (4) and (5), using the estimated parameter Θ_{k+1} (equivalently G_{k+1} and F_{k+1}) from (8), (9), and (11).

C. Parameter Estimation Error Bound and Convergence

Given the fluctuating model parameter Θ_k in the process, the effectiveness of the developed control law in (13) depends on the accuracy of model parameter estimation. The boundedness and convergence of the parameter estimation error are investigated in this section. To analyze the boundedness and convergence of the parameter estimation error, the following notations are used: I denotes the identity matrix of appropriate dimension; $\lambda_{max}(A)$ and $\lambda_{\min}(A)$ represent the maximum and minimum eigenvalues of matrix A, respectively. For real square symmetric matrices A and B, A > B implies that A - B is positive definite.

Following similar treatments in [38], [39], [40], and [41], without loss of generality, in analyzing the boundedness and convergence of parameter estimation error $\Theta_k = \Theta_k - \Theta_k$, we assume the following.

- A1) Measurement noise and parameter uncertainty covariance matrices in (8) and (9) are bounded below and above, i.e., $\underline{\delta}_R I \leq R_k \leq \overline{\delta}_R I$ and $\underline{\delta}_Q I \leq Q_k \leq \overline{\delta}_Q I$, where $\underline{\delta}_{(\cdot)}$ and $\bar{\delta}_{(\cdot)}$ are positive constants.
- A2) The initial parameter estimation error covariance matrix P_0 is symmetric and positive definite.
- A3) There exist a constant $\underline{\delta}_{uu} > 0$ and integers h and j such that

$$\underline{\delta}_{uu}I \le \sum_{i=jh}^{(j+1)h-1} U_i^T U_i \quad \forall j \ge 0, h > 0.$$
 (14)

Given assumptions (A1)–(A3), the following lemmas will be useful in subsequent analysis.

Lemma 1: If there exists a stochastic function $V_k(\zeta_k)$ satisfying the following:

- 1) $\underline{\nu} \|\zeta_k\|^2 \leq V_k(\zeta_k) \leq \overline{\nu} \|\zeta_k\|^2$, where $\underline{\nu}, \overline{\nu} > 0$, 2) $E[V_{k+1}(\zeta_{k+1})|\zeta_k] V_k(\zeta_k) \leq \mu \alpha V_k(\zeta_k)$, where 0 < 0 $\alpha \leq 1$ and $\mu > 0$,

then the variable ζ_k is exponentially bounded in mean square by the following inequality:

$$E[\|\zeta_k\|^2] \le \frac{\bar{\nu}}{\nu} E[\|\zeta_0\|^2] (1-\alpha)^k + \frac{\mu}{\nu} \sum_{i=0}^{k-1} (1-\alpha)^i$$
. Proof: See [42, Th. 2].

Lemma 2: If the estimated parameter vector $\hat{\Theta}_k$ is bounded, equivalently, \hat{G}_k and \hat{F}_k are bounded, then the expectation of the spectral norm of \bar{U}_k or U_k is bounded.

Proof: Control law (13) at k shows

$$\bar{U}_k = (\hat{G}_k^T \hat{G}_k + \kappa I)^{-1} \hat{G}_k^T (Y_d - \hat{F}_k)$$
 (15)

where the term $(\hat{G}_k^T\hat{G}_k+\kappa I)^{-1}\hat{G}_k^T$ can be rewritten using matrix inverse lemma as

$$(\hat{G}_{k}^{T}\hat{G}_{k} + \kappa I)^{-1}\hat{G}_{k}^{T}$$

$$= \kappa^{-1}\hat{G}_{k}^{T} - \kappa^{-1}\hat{G}_{k}^{T}(\kappa^{-1}\hat{G}_{k}\hat{G}_{k}^{T} + I)^{-1}\kappa^{-1}\hat{G}_{k}\hat{G}_{k}^{T}$$

$$= \kappa^{-1}\hat{G}_{k}^{T}(\kappa^{-1}\hat{G}_{k}\hat{G}_{k}^{T} + I)^{-1}.$$
(16)

With (15) and (16), the expectation of the spectrum norm of \bar{U}_k is

$$E\left[\bar{U}_{k}^{T}\bar{U}_{k}\right] = E\left[\kappa^{-2}(Y_{d} - \hat{F}_{k})^{T}(\kappa^{-1}\hat{G}_{k}\hat{G}_{k}^{T} + I)^{-T}\right]$$
$$\hat{G}_{k}\hat{G}_{k}^{T}(\kappa^{-1}\hat{G}_{k}\hat{G}_{k}^{T} + I)^{-1}(Y_{d} - \hat{F}_{k}).$$

As \hat{G}_k is bounded by the projection of parameter estimation, it can be shown that $\kappa^{-1}\hat{G}_k\hat{G}_k^T(\kappa^{-1}\hat{G}_k\hat{G}_k^T+I)^{-1} < I$ and $(\kappa^{-1}\hat{G}_k\hat{G}_k^T+I)^{-1} \leq I$. Then, it can be shown

$$E\left[\bar{U}_k^T \bar{U}_k\right] < E\left[\kappa^{-1} (Y_d - \hat{F}_k)^T (Y_d - \hat{F}_k)\right].$$

Since \hat{F}_k is bounded by the projection of parameter estimation, it implies that control \bar{U}_k is bounded in the mean square.

Defined in (1), U_k is of full row rank, which implies that $U_kU_k^T$ is positive definite and $U_k^TU_k$ is positive semidefinite. Thus, Lemma 2 implies $0 < \underline{\delta}_U I \le U_k U_k^T \le \bar{\delta}_U I$ and $0 \le U_k^T U_k \le \bar{\delta}_U I$, where $\underline{\delta}_U$ and $\bar{\delta}_U$ are positive constants. With the abovementioned prerequisites, the main results are discussed as follows.

Theorem 1: Under assumptions (A1) and (A2), given the system equations (4) and (5) with Kalman parameter estimation from (8), (9), and (11), the parameter estimation error covariance matrix P_k is bounded above and below, i.e.,

$$0 < \delta_P I < P_k < \bar{\delta}_P I < \infty$$

where $0<\underline{\delta}_P<\underline{\delta}_Q$ and $\bar{\delta}_P=p_0+h\bar{\delta}_Q\frac{1-\gamma^{j+1}}{1-\gamma}$. p_0 and γ are given in the proof.

Proof: Substituting L_k in (8) into $I - L_k U_k$ and applying matrix inversion lemma under assumption (A1), it follows:

$$0 \le I - L_k U_k = (I + P_k U_k^T R_k^{-1} U_k)^{-1} \le I.$$
 (17)

Given (17) and assumptions (A1) and (A2), that is, $P_0>0$ and $Q_k\geq\underline{\delta}_QI>0$, it is straightforward to see that using (9) $P_k\geq Q_k\geq\underline{\delta}_QI>0$ for all k, i.e., P_k is bounded below, $P_k>\underline{\delta}_PI$, where $0<\underline{\delta}_P<\underline{\delta}_Q$.

Using (17) and assumptions (A1) and (A3), we have

$$\prod_{i=jh}^{(j+1)h-1} (I + P_i U_i^T R_i^{-1} U_i) > I + \frac{\underline{\delta}_P}{\overline{\delta}_R} \Big(U_{jh}^T U_{jh} + \frac{\underline{\delta}_P}{\overline{\delta}_R} \Big(U_{jh}^T U_{jh} + \frac{\underline{\delta}_P}{\overline{\delta}_R} \Big(U_{jh}^T U_{jh} + \frac{\underline{\delta}_P}{\overline{\delta}_R} \Big) \Big)$$

$$+U_{jh+1}^TU_{jh+1}+U_{jh+2}^TU_{jh+2}+\cdots$$
 $>\left(1+\frac{\underline{\delta}_P\underline{\delta}_{uu}}{\overline{\delta}_R}\right)I>I$

which implies

$$0 \le \lambda \left(\prod_{i=jh}^{(j+1)h-1} (I - L_i U_i) \right) < 1.$$
 (18)

Enumerating (9) and using assumption (A1), we have

$$P_{k} \leq \left[\prod_{i=1}^{k-1} (I - L_{i}U_{i}) \right] P_{0} + \left[I + \prod_{i=k-1}^{k-1} (I - L_{i}U_{i}) + \prod_{i=k-2}^{k-1} (I - L_{i}U_{i}) + \cdots + \prod_{i=1}^{k-1} (I - L_{i}U_{i}) \right] \bar{\delta}_{Q} I.$$
 (19)

Applying the result in (18), (19) becomes

$$\begin{split} P_k &< P_0 + \left[I + \prod_{i=k-1}^{k-1} (I - L_i U_i) + \dots + \prod_{i=k-h+1}^{k-1} (I - L_i U_i) \right. \\ &+ \prod_{i=k-h}^{k-1} (I - L_i U_i) + \dots + \prod_{i=k-h}^{k-1} \prod_{i=k-2h+1}^{k-h-1} (I - L_i U_i) \\ &+ \dots + \prod_{i=k-h}^{k-1} \prod_{i=k-2h}^{k-h-1} \dots \prod_{i=k-jh}^{k-(j-1)h-1} (I - L_i U_i) + \dots \\ &+ \prod_{i=k-h}^{k-1} \prod_{i=k-2h}^{k-h-1} \dots \prod_{i=k-jh}^{k-(j-1)h-1} \prod_{i=1}^{k-jh-1} (I - L_i U_i) \right] \bar{\delta}_Q \\ &\leq P_0 + \left[h + h\gamma + h\gamma^2 + \dots + h\gamma^j \right] \bar{\delta}_Q I \\ &\leq \left(p_0 + h\bar{\delta}_Q \frac{1 - \gamma^{j+1}}{1 - \gamma} \right) I \end{split}$$

where $\gamma = \lambda_{\max} \left\{ \prod_{i=k-h}^{k-1} (I - L_i U_i), \prod_{i=k-2h}^{k-h-1} (I - L_i U_i), \ldots, \prod_{i=k-jh}^{k-(j-1)h-1} (I - L_i U_i) \right\} < 1, p_0 = \lambda_{\max}(P_0), \text{ and } j \text{ is the quotient of } (k/h).$

By choosing $0 < \underline{\delta}_P < \underline{\delta}_Q$ and $\bar{\delta}_P = p_0 + h\bar{\delta}_Q \frac{1-\gamma^{j+1}}{1-\gamma}$, the proof is complete.

Theorem 2: Given Lemmas 1–2, Theorem 1, and assumption (A1), the parameter estimation error $\tilde{\Theta}_k$ is exponentially bounded in mean square.

Proof: Since P_k is shown to be positive definite and bounded in Theorem 1, we introduce a Lyapunov function candidate

$$V_k = \tilde{\Theta}_k^T P_k^{-1} \tilde{\Theta}_k.$$

Subtracting (7) from (4), the parameter estimation error at k+1 is

$$\tilde{\Theta}_{k+1} = (I - L_k U_k) \tilde{\Theta}_k + \mathbf{w}_{k+1} - L_k \mathbf{v}_k.$$

Substituting $\tilde{\Theta}_{k+1}$ into V_{k+1} and taking the conditional expectation with respect to $\tilde{\Theta}_k$, we have

$$E[V_{k+1}|\tilde{\Theta}_{k}] = E[\tilde{\Theta}_{k+1}^{T} P_{k+1}^{-1} \tilde{\Theta}_{k+1} | \tilde{\Theta}_{k}]$$

$$= \tilde{\Theta}_{k}^{T} (I - L_{k} U_{k})^{T} P_{k+1}^{-1} (I - L_{k} U_{k}) \tilde{\Theta}_{k}$$

$$+ E[\mathbf{w}_{k+1}^{T} P_{k+1}^{-1} \mathbf{w}_{k+1}] + E[\mathbf{v}_{k}^{T} L_{k}^{T} P_{k+1}^{-1} L_{k} \mathbf{v}_{k}].$$
(20)

The parameter estimation error covariance matrix P_{k+1} can be written as follows:

$$P_{k+1} = E[\tilde{\Theta}_{k+1}\tilde{\Theta}_{k+1}^T]$$

$$= (I - L_k U_k) P_k (I - L_k U_k)^T + Q_{k+1} + L_k R_k L_k^T.$$
(21)

From assumption (A1) $R_k > 0$, which implies $L_k R_k L_k^T \ge 0$. Hence, (21) becomes

$$P_{k+1} \ge (I - L_k U_k) P_k (I - L_k U_k)^T + Q_{k+1}. \tag{22}$$

Since P_k is shown to be bounded in Theorem 1, (17) implies $0 < (I - L_k U_k) \le I$. Using assumption (A1), we can rewrite (22) as

$$P_{k+1} \ge (I - L_k U_k) P_k (I - L_k U_k)^T + (I - L_k U_k) (I - L_k U_k)^{-1} Q_{k+1} (I - L_k U_k)^{-T} (I - L_k U_k)^T$$

$$\ge (I - L_k U_k) (P_k + \delta_O I) (I - L_k U_k)^T.$$
(23)

Taking inverse on both sides of (23) and substituting the result into the first term on the right-hand side of (20), we have

$$\tilde{\Theta}_k^T (I - L_k U_k)^T P_{k+1}^{-1} (I - L_k U_k) \tilde{\Theta}_k \le \tilde{\Theta}_k^T (P_k + \underline{\delta}_Q I)^{-1} \tilde{\Theta}_k.$$
(24)

Using matrix inversion lemma, (24) can be written as

$$\tilde{\Theta}_{k}^{T}(P_{k} + \underline{\delta}_{Q}I)^{-1}\tilde{\Theta}_{k} < \left(1 - \frac{\underline{\delta}_{Q}\underline{\delta}_{P}}{\overline{\delta}_{P}(\underline{\delta}_{Q} + \underline{\delta}_{P})}\right)\tilde{\Theta}_{k}^{T}P_{k}^{-1}\tilde{\Theta}_{k}.$$
(25)

Letting $\alpha=\frac{\underline{\delta}_Q\underline{\delta}_P}{\bar{\delta}_P(\underline{\delta}_Q+\underline{\delta}_P)}$ in (25), we have

$$\tilde{\Theta}_{k}^{T}(I - L_{k}U_{k})^{T} P_{k+1}^{-1}(I - L_{k}U_{k})\tilde{\Theta}_{k} < (1 - \alpha)V_{k}.$$
 (26)

Using matrix inversion lemma, we have

$$P_{k+1} = (P_k^{-1} + U_k^T R_k^{-1} U_k)^{-1} + Q_{k+1}$$

> $(P_k^{-1} + U_k^T R_k^{-1} U_k)^{-1}$. (27)

Taking inverse on both sides of (27), we get

$$L_k^T P_{k+1}^{-1} L_k < L_k^T \left(P_k^{-1} + U_k^T R_k^{-1} U_k \right) L_k. \tag{28}$$

Substituting (8) into (28), it follows:

$$L_k^T P_{k+1}^{-1} L_k < \left(\frac{\bar{\delta}_P \bar{\delta}_U \underline{\delta}_R + \bar{\delta}_P^2 \bar{\delta}_U^2}{\underline{\delta}_R (\underline{\delta}_U \underline{\delta}_P + \underline{\delta}_R)^2}\right) I. \tag{29}$$

With (27) and (29), the second and third terms on the right-hand side of (20) can be written as

$$E[\mathbf{w}_{k+1}^T P_{k+1}^{-1} \mathbf{w}_{k+1}] < \left(\frac{1}{\underline{\delta}_P} + \frac{\delta_U}{\underline{\delta}_R}\right) E[\mathbf{w}_{k+1}^T \mathbf{w}_{k+1}] \text{ and}$$

$$E[\mathbf{v}_k^T L_k^T P_{k+1}^{-1} L_k \mathbf{v}_k] < \left(\frac{\overline{\delta}_P \overline{\delta}_U \underline{\delta}_R + \overline{\delta}_P^2 \overline{\delta}_U^2}{\delta_R (\delta_U \delta_P + \delta_P)^2}\right) E[\mathbf{v}_k^T \mathbf{v}_k]. \tag{30}$$

Assumption (A1) shows that $R_k = E[\mathbf{v}_k \mathbf{v}_k^T] \leq \bar{\delta}_R I$ and $Q_k = E[\mathbf{w}_k \mathbf{w}_k^T] \leq \bar{\delta}_Q I$, which implies that $E[\mathbf{w}_{k+1}^T \mathbf{w}_{k+1}] \leq \bar{\delta}_Q m$ and $E[\mathbf{v}_k^T \mathbf{v}_k] \leq \bar{\delta}_R n$, where m is the dimension of the parameter to be estimated and n is the dimension of the output.

Incorporating (26) and (30), (20) becomes

$$E[V_{k+1}|\tilde{\Theta}_k] < (1-\alpha)V_k + \left(\frac{1}{\underline{\delta}_P} + \frac{\bar{\delta}_U}{\underline{\delta}_R}\right)\bar{\delta}_Q m + \left(\frac{\bar{\delta}_P\bar{\delta}_U\underline{\delta}_R + \bar{\delta}_P^2\bar{\delta}_U^2}{\underline{\delta}_R(\underline{\delta}_U\underline{\delta}_P + \underline{\delta}_R)^2}\right)\bar{\delta}_R n$$
(31)

where $\alpha = \frac{\underline{\delta_Q}\underline{\delta_P}}{\overline{\delta_P}(\underline{\delta_Q} + \underline{\delta_P})} < 1$ and positive. Since the constructed Lyapunov function and (31) satisfy the conditions of Lemma 1, the parameter estimation error $\tilde{\Theta}_k$ is exponentially bounded in mean square.

Theorems 1 and 2 ensure the boundedness and convergence of the parameter estimation error using Kalman estimator for the given stochastic process equations (4) and (5), and consequently justify the fidelity of the developed controller. These results are required for analyzing closed-loop stability.

D. Stability Analysis

To account for system uncertainties, which are presented as random variables in the derived stochastic plant model equations (4) and (5), following the similar fashion in [43] and [44], the stability of the closed-loop system is analyzed by bounding the control input, the system output, and the tracking error Ξ_k in the mean square sense.

Theorem 3: Consider a stochastic plant model equations (4) and (5) and a projection-based Kalman estimation algorithm for its parameter estimation given in (8), (9), and (11). Using the proposed control law in (13), if the estimated model parameter $\hat{\Theta}_k$ (or equivalently \hat{G}_k and \hat{F}_k) is bounded and its estimation error $\tilde{\Theta}_k$ (or equivalently \tilde{G}_k and \tilde{F}_k) is exponentially bounded in the mean square, with the assumption (A1), the control input \bar{U}_k , system output Y_k , and tracking error Ξ_k are bounded in the sense of mean square, and closed-loop system is stable.

Proof: Substituting the control law (13) at the instant k into the system (5), we have

$$Y_k = \kappa^{-1} (\hat{G}_k + \tilde{G}_k) \hat{G}_k^T (\kappa^{-1} \hat{G}_k \hat{G}_k^T + I)^{-1} (Y_d - \hat{F}_k)$$

$$+ F_k + \nu_k.$$
(32)

Because the estimated parameters are bounded by the projection, it can be seen that $\kappa^{-\frac{1}{2}}\hat{G}_k^T(\kappa^{-1}\hat{G}_k\hat{G}_k^T+I)^{-1} < I$ and $\kappa^{-1}\hat{G}_k\hat{G}_k^T(\kappa^{-1}\hat{G}_k\hat{G}_k^T+I)^{-1} < I$. Using these inequalities, (32) becomes

$$Y_k < Y_d + \kappa^{-\frac{1}{2}} \tilde{G}_k (Y_d - \hat{F}_k) + \tilde{F}_k + \nu_k.$$
 (33)

Considering the output Y_k in the mean square sense, with the inequality (33), we have

$$E\left[Y_{k}^{T}Y_{k}\right] < E\left[\left(Y_{d} + \kappa^{-\frac{1}{2}}\tilde{G}_{k}(Y_{d} - \hat{F}_{k}) + \tilde{F}_{k} + \nu_{k}\right)^{T} \left(Y_{d} + \kappa^{-\frac{1}{2}}\tilde{G}_{k}(Y_{d} - \hat{F}_{k}) + \tilde{F}_{k} + \nu_{k}\right)\right]$$

$$= E\left[Y_{d}^{T}Y_{d} + 2\kappa^{-\frac{1}{2}}Y_{d}^{T}\tilde{G}_{k}(Y_{d} - \hat{F}_{k}) + 2Y_{d}^{T}\tilde{F}_{k} + \kappa^{-1}(Y_{d} - \hat{F}_{k})^{T}\tilde{G}_{k}^{T}\tilde{G}_{k}(Y_{d} - \hat{F}_{k}) + 2\kappa^{-\frac{1}{2}}(Y_{d} - \hat{F}_{k})^{T}\tilde{G}_{k}^{T}\tilde{F}_{k} + \tilde{F}_{k}^{T}\tilde{F}_{k} + \nu_{k}^{T}\nu_{k}\right]. \tag{34}$$

Using (32), the tracking error is

$$\Xi_{k} = Y_{d} - Y_{k} = Y_{d} - G_{k}\bar{U}_{k} - F_{k} - \nu_{k}$$

$$= \left(I - \kappa^{-1}G_{k}\hat{G}_{k}^{T}(\kappa^{-1}\hat{G}_{k}\hat{G}_{k}^{T} + I)^{-1}\right)(Y_{d} - \hat{F}_{k}) - \tilde{F}_{k} - \nu_{k}$$
(35)

where we have

$$I - \kappa^{-1} G_k \hat{G}_k^T (\kappa^{-1} \hat{G}_k \hat{G}_k^T + I)^{-1}$$

$$= (I - \kappa^{-1} \tilde{G}_k \hat{G}_k^T) (I + \kappa^{-1} \hat{G}_k \hat{G}_k^T)^{-1} \le I - \kappa^{-1} \tilde{G}_k \hat{G}_k^T.$$
(36)

Considering the tracking error Ξ_k in the mean square sense, with (35) and (36), we have

$$E[\Xi_{k}^{T}\Xi_{k}] \leq E\left[\left((Y_{d} - \hat{F}_{k})^{T}(I - \kappa^{-1}\tilde{G}_{k}\hat{G}_{k}^{T})^{T} - \tilde{F}_{k}^{T} - \nu_{k}^{T}\right)\right]$$

$$\left(\left(I - \kappa^{-1}\tilde{G}_{k}\hat{G}_{k}^{T}\right)(Y_{d} - \hat{F}_{k}) - \tilde{F}_{k} - \nu_{k}\right)\right]$$

$$= E\left[(Y_{d} - \hat{F}_{k})^{T}(I - \kappa^{-1}\tilde{G}_{k}\hat{G}_{k}^{T})^{T}(I - \kappa^{-1}\tilde{G}_{k}\hat{G}_{k}^{T})(Y_{d} - \hat{F}_{k}) - 2(Y_{d} - \hat{F}_{k})^{T}(I - \kappa^{-1}\tilde{G}_{k}\hat{G}_{k}^{T})\tilde{F}_{k} + \tilde{F}_{k}^{T}\tilde{F}_{k} + \nu_{k}^{T}\nu_{k}\right].$$
(37)

Equations (34) and (37) disclose that the boundedness and convergence of the mean squares of output Y_k and tracking error Ξ_k are determined by these of the estimated parameters, \tilde{G}_k and \hat{F}_k , the estimation errors, \tilde{G}_k and \tilde{F}_k , the desired output Y_d , and the measurement noise ν_k . With the result of Theorem 2, Lemma 2, which shows that the mean square of control input \bar{U}_k is bounded, and the projection for bounding the estimated parameters, we conclude that the closed-loop system is bounded-input bounded-output stable with the proposed control algorithm.

Remark 3: Similar to indirect adaptive control, the proposed parameter estimation and control algorithms do not require nor ensure all estimated parameters converge to their true values.

IV. EXPERIMENTAL VALIDATION

A. Experiment Implementation

In total, six open-loop experiments were conducted using the same nozzle with the same jetting control parameter pair (u_1, u_2) at different dates and times. In each experiment, 1000 drops were imaged at drop printing frequency of 2 Hz with stroke velocity

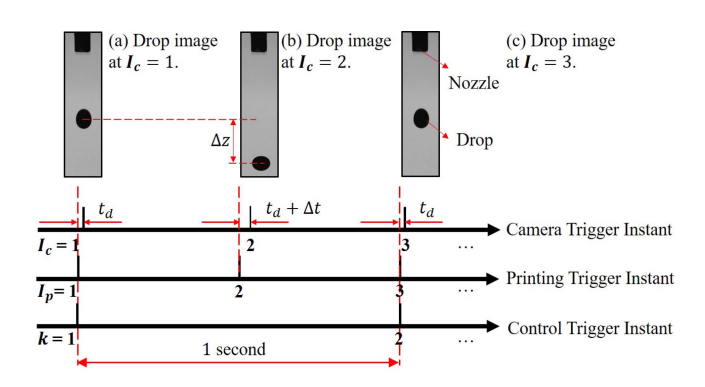


Fig. 6. Schematic of trigger timings for sampling a drop image, firing a drop, and updating the control input.

 $u_1=63.27~\mu\mathrm{m}/\mathrm{ms}$ and stroke $u_2=21.69~\mu\mathrm{m}$, which were determined based on the nominal model parameters listed in (2) to generate the target output $Y_d=[y_d^{\mathrm{vol}}~y_d^{\mathrm{vel}}]^T=[15~\mathrm{nl}~0.8~\mathrm{m/s}]^T.$ Fig. 6 shows the trigger timings to the camera to sample a drop image, to the printhead to fire a drop, and to the controller to update the control action. A trigger delay t_d sent to the strobe LED was adjusted until a well-defined discrete drop was observed in flight. Drop jetting velocity was calculated from two consecutive drop samples at the odd and even instants. An additional delay time Δt was applied to the LED at the even instant to image the in-flight drop at Δt after the odd camera sampling instant so that the backward difference can be used to approximate the drop jetting velocity, i.e., $y^{\mathrm{vel}} = \Delta z/\Delta t$, where Δz is the difference of centroids of two drops, as shown in Fig. 6. Drop volumes of the odd sampled drops were computed [24].

To implement the proposed control strategy, the covariance matrices of the process parameter uncertainty Q_k and the measurement noise R_k of the Kalman estimator have to be determined. Since it is not practical to image the same drop at the same displacement away from the nozzle multiple times while the image capture system is stationary, we assume that the measurement noise \mathbf{v}_k is stationary and its covariance R can be approximated by its time samples. An open-loop experiment dataset was used to determine the measurement noise covariance R as follows:

$$\begin{split} R &= \begin{bmatrix} \text{cov}(y^{\text{vol}}, y^{\text{vol}}) & \text{cov}(y^{\text{vol}}, y^{\text{vel}}) \\ \text{cov}(y^{\text{vel}}, y^{\text{vol}}) & \text{cov}(y^{\text{vel}}, y^{\text{vel}}) \end{bmatrix} \\ &= \begin{bmatrix} 0.01 & 0.00007 \\ 0.00007 & 0.00002 \end{bmatrix} \end{split}$$

where $cov(\cdot,\cdot)$ is the covariance of two vectors of random variables

An innovation-based adaptive algorithm [45] was used to estimate the covariance Q_k of the parameter uncertainty \mathbf{w}_k in (5), where

$$\hat{Q}_k = L_k \Psi L_k^T \tag{38}$$

and Ψ was calculated from

$$\Psi = \frac{1}{N} \sum_{i=k-N+1}^{k} \psi_i \psi_i^T.$$
 (39)

In the abovementioned equation, N is the moving window size, which was set to 5. The innovation sequence ψ_i is the difference between the measured output and the estimated output

$$\psi_i = Y_i - U_i \hat{\Theta}_i. \tag{40}$$

To compare with the performance of the proposed control strategy, a widely used integral control (I-controller) [22]

$$\bar{U}_{k+1} = \bar{U}_k + K_I \Xi_k \tag{41}$$

was implemented. In (41), Ξ_k is the tracking error at the instant k. The integral gain K_I was selected by inverting the nominal model in (2) to achieve the best nominal performance, i.e.,

$$K_I = G_o^{-1}$$
.

The nominal model parameters in (2) were used to initialize the Kalman estimation algorithm.

To validate the effectiveness of the proposed control strategy, closed-loop control experiments were conducted with

- 1) *I-controller*—the integral controller, see (41),
- 2) proposed controller—the proposed controller described by (13), where κ was set to 0.000001.

Maximum and minimum values of the control input, \bar{U}_{max} and \bar{U}_{min} , were set to the upper and lower limits of the control parameters used in data collection, as shown in Fig. 3, where

$$\begin{cases} \bar{U}_k = \bar{U}_{\text{max}} & \text{if } \bar{U}_k \ge \bar{U}_{\text{max}} \\ \bar{U}_k = \bar{U}_{\text{min}} & \text{if } \bar{U}_k \le \bar{U}_{\text{min}} \\ \bar{U}_k = \bar{U}_k & \text{otherwise.} \end{cases}$$
(42)

The closed-loop experiments used the same procedure as the open-loop tests, while the calculated drop volume and jetting velocity were fed back to update the control input, the firing parameters (u_1, u_2) , once a second, see instant k in Fig. 6.

B. Experimental Results

When analyzing the experimental results, the first ten transient samples were removed, which is in agreement with the industrial printing operating procedure, where a printhead is routinely primed before printing to remove the "first drop problem" [46], [47].

Open-loop outputs shown in Fig. 1 were plotted in scatter graphs in gray, see Fig. 7. Although the constant control input, which was calculated from the nominal model to deliver the target outputs, was used, the open-loop results spread widely and deviate from the center of the plot, which denotes the target outputs. The corresponding histograms of drop volume and drop jetting velocity show that the open-loop results exhibit a large dispersion. Table I confirms that the open-loop results have a mean value of 14.41 nl for drop volume and 0.82 m/s for drop jetting velocity, which are away from the targets. Large RSDs are presented as expected. The open-loop drop volume has an RSD of 3.23%, and the RSD of the drop jetting velocity is 2.56%.

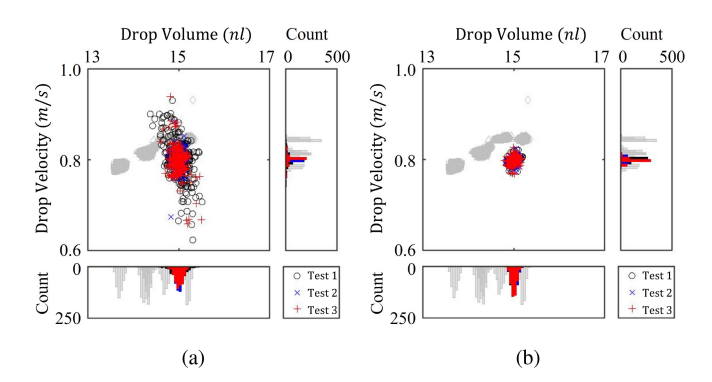


Fig. 7. System outputs using the (a) I-controller and (b) proposed controller, respectively, for three different tests conducted at different times. Gray markers are open-loop outputs. Color markers are controlled outputs.

TABLE I STATISTICS OF OPEN-LOOP AND CONTROLLED DROP VOLUMES (NL) AND DROP JETTING VELOCITIES (M/S)

Feature	Method	Mean	RSD
Drop Volume	Open loop	14.41	3.23 %
	I-controller	15.00	0.77 %
	Proposed controller	15.00	0.42 %
Drop Jetting Velocity	Open loop	0.82	2.56 %
	I-controller	0.80	3.25 %
	Proposed controller	0.80	0.75 %

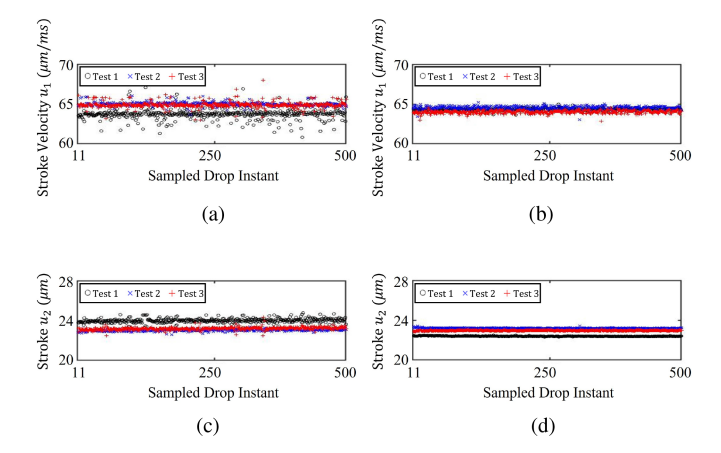


Fig. 8. System control inputs, stroke velocity u_1 , and stroke u_2 , using the I-controller and proposed controller, respectively, for three different tests conducted at different times. (a) I-controller: Stroke velocity u_1 . (b) Proposed controller: Stroke velocity u_1 . (c) I-controller: Stroke u_2 . (d) Proposed controller: Stroke u_2 .

The color markers in Fig. 7 represent the controlled drop volume and jetting velocity of three tests conducted at different times using the I-controller and the proposed controller, respectively. The I-controller controlled outputs show a larger spread although they are around the center of the plot [see Fig. 7(a)]. Fig. 7(b) shows that the closed-loop outputs using the proposed controller are convergent to the targets with tight variances, where the spread of drop jetting velocity is reduced tremendously. In the associated histograms, it can be seen that the majority of sampled drops have the desired characteristics.

Table I compares the statistics of the controlled results. The mean values of the controlled drop volume and drop jetting velocity are equal to the target values, 15 nl and 0.8 m/s, for

all controllers, which validate their effectiveness in achieving the prescribed tracking performance. Table I also shows that the proposed control strategy is superior in reducing output variance than the I-controller. Although the RSD of the drop volume controlled by the I-controller is a fourth of that of the open-loop drop volume, the I-controller deteriorates the drop jetting velocity, resulting in a higher RSD. By contrast, the proposed controller is able to narrow down the RSDs of both drop volume and drop jetting velocity.

Drop volumes of the other 500 controlled drops sampled at even instants, which were not used for control update, were also calculated for each controller. Their statistics show RSDs comparable to the results shown in Table I and less than 2% errors in the mean, which are primarily contributed by the volume estimation error due to uneven back illuminance.

Control parameters, stroke velocity u_1 and stroke u_2 , are shown in Fig. 8. As implied in the plant model, the control input and the system output are stochastically correlated. Less fluctuating control inputs of the proposed controller result in narrower output spreads, while both outputs and inputs of the I-controller have relatively larger variations. This suggests that implementing a boundary layer around the control input may further reduce output fluctuations.

V. CONCLUSION AND DISCUSSION

This article proposed a closed-loop drop volume and jetting velocity control using one-step look ahead projection-based Kalman estimation. The proposed approach used standard printhead calibration data to identify regression-like affine models with stochastic parameters for control synthesis. Experimental results validate the effectiveness of the proposed approach, and associated system stability and parameter convergence are analyzed. This modeling and control framework can be employed for different inkjet printhead architectures and, in turn, can be widely applied to different industrial-level DoD inkjet printing processes. The sample rate of the proposed control strategy and, in turn, the resulting jetting frequency are limited by the camera frame rate and the image analysis computation time. Although the implementation of the proposed control strategy was done at a relatively low firing rate in this work, it can be increased with better processing hardware, such as GPU or FPGA, or with a higher frame rate camera. Another option to implement the proposed approach at higher jetting frequencies is to sample the drops at a lower rate. This results in open-loop control for drops that are between samples. In this case, the proposed approach is only able to address low bandwidth fluctuations and slow drifts, which are characteristics of disturbances in inkjet printing associated with changes in ambient conditions and ink property fluctuation.

REFERENCES

- M. Alomari, F. H. Mohamed, A. W. Basit, and S. Gaisford, "Personalized dosing: Printing a dose of one's own medicine," *Int. J. Pharmaceutics*, vol. 494, no. 2, pp. 568–577, 2015.
- [2] N. Bajaj, J. F. Rhoads, and G. T. -C. Chiu, "Characterizing the spatially dependent sensitivity of resonant mass sensors using inkjet deposition," J. Dyn. Syst. Meas. Control, vol. 139, no. 11, 2017, Art. no. 114505.

- [3] J. Lessing, A. C. Glavan, S. B. Walker, C. Keplinger, J. A. Lewis, and G. M. Whitesides, "Inkjet printing of conductive inks with high lateral resolution on omniphobic "R^F paper" for paper-based electronics and mems," Adv. Mater., vol. 26, no. 27, pp. 4677–4682, 2014.
- [4] A. K. Murray et al., "Selectively-deposited energetic materials: A feasibility study of the piezoelectric inkjet printing of nanothermites," *Additive Manuf.*, vol. 22, pp. 69–74, 2018.
- [5] Q. Xu and O. A. Basaran, "Computational analysis of drop-on-demand drop formation," *Phys. Fluids*, vol. 19, no. 10, 2007, Art. no. 102111.
- [6] H. Wijshoff, "The dynamics of the Piezo inkjet printhead operation," *Phys. Rep.*, vol. 491, no. 4, pp. 77–177, 2010.
- [7] J. Castrejón-Pita, N. Morrison, O. Harlen, G. Martin, and I. Hutchings, "Experiments and Lagrangian simulations on the formation of droplets in drop-on-demand mode," *Phys. Rev. E*, vol. 83, 2011, Art. no. 036306.
- [8] Y. Liu and B. Derby, "Experimental study of the parameters for stable drop-on-demand inkjet performance," *Phys. Fluids*, vol. 31, no. 3, 2019, Art. no. 032004.
- [9] J. Chang, Y. Liu, and B. Huang, "Effects of dwell time of excitation waveform on meniscus movements for a tubular piezoelectric print-head: Experiments and model," *J. Micromechanics Microeng.*, vol. 27, no. 7, 2017, Art. no. 075023.
- [10] R. Haas, S. Lohse, C. E. Düllmann, K. Eberhardt, C. Mokry, and J. Runke, "Development and characterization of a drop-on-demand inkjet printing system for nuclear target fabrication," *Nucl. Instruments Methods Phys. Res. Sect. A: Accelerators, Spectrometers, Detectors Assoc. Equip.*, vol. 874, pp. 43–49, 2017.
- [11] D. Zhao, H. Zhou, Y. Wang, J. Yin, and Y. Huang, "Drop-on-demand (DoD) inkjet dynamics of printing viscoelastic conductive ink," *Additive Manuf.*, vol. 48, 2021, Art. no. 102451.
- [12] H. Y. Gan, X. Shan, T. Eriksson, B. K. Lok, and Y. C. Lam, "Reduction of droplet volume by controlling actuating waveforms in inkjet printing for micro-pattern formation," *J. Micromechanics Microeng.*, vol. 19, no. 5, 2009, Art. no. 055010.
- [13] P. Shin, J. Sung, and M. H. Lee, "Control of droplet formation for low viscosity fluid by double waveforms applied to a piezoelectric inkjet nozzle," *Microelectronics Rel.*, vol. 51, no. 4, pp. 797–804, 2011.
- [14] O. Oktavianty, T. Kyotani, S. Haruyama, and K. Kaminishi, "New actuation waveform design of DoD inkjet printer for single and multi-drop ejection method," *Additive Manuf.*, vol. 25, pp. 522–531, 2019.
- [15] A. A. Khalate, X. Bombois, R. Babuška, H. Wijshoff, and R. Waarsing, "Performance improvement of a drop-on-demand inkjet printhead using an optimization-based feedforward control method," *Control Eng. Pract.*, vol. 19, no. 8, pp. 771–781, 2011.
- [16] A. A. Khalate, X. Bombois, S. Ye, R. Babuška, and S. Koekebakker, "Minimization of cross-talk in a piezo inkjet printhead based on system identification and feedforward control," *J. Micromechanics Microeng.*, vol. 22, no. 11, 2012, Art. no. 115035.
- [17] M. Ezzeldin, P. van den Bosch, and S. Weiland, "Experimental-based feedforward control for a DoD inkjet printhead," *Control Eng. Pract.*, vol. 21, no. 7, pp. 940–952, 2013.
- [18] J. Yun et al., "Droplet property optimization in printable electronics fabrication using root system growth algorithm," *Comput. Ind. Eng.*, vol. 125, pp. 592–603, 2018.
- [19] B. Snyder, M. Yang, S. Singhal, O. Abed, and S. Sreenivasan, "Automated tuning of high-order waveforms for picoliter resolution jetting of rheologically challenging materials," *Precis. Eng.*, vol. 56, pp. 143–155, 2019.
- [20] N. Genina, D. Fors, M. Palo, J. Peltonen, and N. Sandler, "Behavior of printable formulations of loperamide and caffeine on different substrates effect of print density in inkjet printing," *Int. J. Pharmaceutics*, vol. 453, no. 2, pp. 488–497, 2013.
- [21] O. Kiefer, B. Fischer, and J. Breitkreutz, "Fundamental investigations into metoprolol tartrate deposition on orodispersible films by inkjet printing for individualised drug dosing," *Pharmaceutics*, vol. 13, no. 2, 2021, Art. no. 247.
- [22] K. Barton, S. Mishra, A. Alleyne, P. Ferreira, and J. Rogers, "Control of high-resolution electrohydrodynamic jet printing," *Control Eng. Pract.*, vol. 19, no. 11, pp. 1266–1273, 2011.
- [23] T. Wang, T.-H. Kwok, C. Zhou, and S. Vader, "In-situ droplet inspection and closed-loop control system using machine learning for liquid metal jet printing," J. Manuf. Syst., vol. 47, pp. 83–92, 2018.
- [24] J. Wang, X. Chen, and G. Chiu, "Drop volume control in drop-on-demand inkjet printing," in *Proc. ASME Dyn. Syst. Control Conf.*, vol. 3, Oct. 2019, Art. no. V003T17A011.
- [25] J. Wang and G. T. -C. Chiu, "Control of drop volume and drop jetting velocity in inkjet printing," in *Proc. 9th IFAC Symp. Mechatronic Syst.*, 2022, vol. 55, no. 27, pp. 37–43.

- [26] J. Wang and G. T.- C. Chiu, "Data-driven drop formation modeling in nanoliter drop-on-demand inkjet printing," in *Proc. ASME Dyn. Syst. Control Conf.*, vol. 2, Oct. 2020, Art. no. V002T28A002.
- [27] W. Streule, T. Lindemann, G. Birkle, R. Zengerle, and P. Koltay, "Pipejet: A simple disposable dispenser for the nano- and microliter range," *J. Assoc. Lab. Automat.*, vol. 9, no. 5, pp. 300–306, 2004.
- [28] L. Zanni, J.-Y. Le Boudec, R. Cherkaoui, and M. Paolone, "A predictionerror covariance estimator for adaptive Kalman filtering in step-varying processes: Application to power-system state estimation," *IEEE Trans. Control Syst. Technol.*, vol. 25, no. 5, pp. 1683–1697, Sep. 2017.
- [29] C. Johnson and E. Tse, "Adaptive implementation of one-step-ahead optimal control via input matching," *IEEE Trans. Autom. Control*, vol. 23, no. 5, pp. 865–872, Oct. 1978.
- [30] G. Goodwin, C. Johnson, and K. Sin, "Global convergence for adaptive one-step-ahead optimal controllers based on input matching," *IEEE Trans. Autom. Control*, vol. 26, no. 6, pp. 1269–1273, Dec. 1981.
- [31] K. Lo and D. Zhang, "Stochastic adaptive one-step-ahead optimal controllers based on input matching," *IEEE Trans. Autom. Control*, vol. 45, no. 5, pp. 980–983, May 2000.
- [32] A. Kiruluta, M. Eizenman, and S. Pasupathy, "Predictive head movement tracking using a Kalman filter," *IEEE Trans. Systems, Man, Cybernet. Part B.*, vol. 27, no. 2, pp. 326–331, Apr. 1997.
- [33] E. Palmer, W. Pen, and C. Spanos, "Control of photoresist properties: A Kalman filter based approach," *IEEE Trans. Semicond. Manuf.*, vol. 9, no. 2, pp. 208–214, May 1996.
- [34] K. J. Åström and B. Wittenmark, "Problems of identification and control," J. Math. Anal. Appl., vol. 34, no. 1, pp. 90–113, 1971.
- [35] P. A. Ioannou and J. Sun, Robust Adaptive Control. Upper Saddle River, NJ, USA: PTR Prentice-Hall, 1996.
- [36] H. Fujimoto and B. Yao, "Multirate adaptive robust control for discrete-time non-minimum phase systems and application to linear motors," IEEE/ASME Trans. Mechatron., vol. 10, no. 4, pp. 371–377, Aug. 2005.

- [37] G. C. Goodwin and K. S. Sin, Adaptive Filtering, Prediction and Control. Englewood Cliffs, NJ, USA: Prentice-Hall, 1984.
- [38] A. H. Jazwinski, Stochastic Processes and Filtering Theory. Cambridge, MA, USA: Academic Press, 1970.
- [39] B. D. O. Anderson and J. B. Moore, "Detectability and stabilizability of time-varying discrete-time linear systems," SIAM J. Control Optim., vol. 19, no. 1, pp. 20–32, 1981.
- [40] L. Guo, "Estimating time-varying parameters by the Kalman filter based algorithm: Stability and convergence," *IEEE Trans. Autom. Control*, vol. 35, no. 2, pp. 141–147, Feb. 1990.
- [41] K. Reif, S. Gunther, E. Yaz, and R. Unbehauen, "Stochastic stability of the discrete-time extended Kalman filter," *IEEE Trans. Autom. Control*, vol. 44, no. 4, pp. 714–728, Apr. 1999.
- [42] T.-J. Tarn and Y. Rasis, "Observers for nonlinear stochastic systems," *IEEE Trans. Autom. Control*, vol. 21, no. 4, pp. 441–448, Aug. 1976.
- [43] G. C. Goodwin, P. J. Ramadge, and P. E. Caines, "Discrete time stochastic adaptive control," SIAM J. Control Optim., vol. 19, no. 6, pp. 829–853, 1981.
- [44] P. Kumar, "Convergence of adaptive control schemes using least-squares parameter estimates," *IEEE Trans. Autom. Control*, vol. 35, no. 4, pp. 416–424, Apr. 1990.
- [45] A. H. Mohamed and K. P. Schwarz, "Adaptive Kalman filtering for INS/GPS," J. Geodesy, vol. 73, no. 4, pp. 193–203, 1999.
- [46] C. Taylor, R. H. Lewis, and A. Murcia, "Printer and method for priming an inkjet printhead," U.S. Patent 6419343B1, Jul. 16, 2002.
- [47] A. Famili, S. A. Palkar, and W. J. Baldy, "First drop dissimilarity in drop-on-demand inkjet devices," *Phys. Fluids*, vol. 23, no. 1, 2011, Art. no. 012109.